

Article

Strain Engineering in Ni-Co-Mn-Sn Magnetic Shape Memory Alloys: Influence on the Magnetic Properties and Martensitic Transformation

Qinhan Xia ¹, Changlong Tan ^{1,2,*}, Binglun Han ¹, Xiaohua Tian ^{3,*}, Lei Zhao ², Wenbin Zhao ², Tianyou Ma ¹, Cheng Wang ¹ and Kun Zhang ^{1,2,4,*}

¹ School of Science, Harbin University of Science and Technology, Harbin 150080, China

² School of Materials Science and Chemical Engineering, Harbin University of Science and Technology, Harbin 150080, China

³ School of Electrical and Electronic Engineering, Harbin University of Science and Technology, Harbin 150080, China

⁴ Shenyang National Laboratory for Materials Science, Institute of Metal Research, Chinese Academy of Sciences, Shenyang 110016, China

* Correspondence: changlongtan@hrbust.edu.cn (C.T.); xiaohuatian@hrbust.edu.cn (X.T.); kunzhang@hrbust.edu.cn (K.Z.)



Citation: Xia, Q.; Tan, C.; Han, B.; Tian, X.; Zhao, L.; Zhao, W.; Ma, T.; Wang, C.; Zhang, K. Strain Engineering in Ni-Co-Mn-Sn Magnetic Shape Memory Alloys: Influence on the Magnetic Properties and Martensitic Transformation. *Materials* **2022**, *15*, 5889. <https://doi.org/10.3390/ma15175889>

Academic Editor: Francesco Iacoviello

Received: 16 July 2022

Accepted: 23 August 2022

Published: 26 August 2022

Publisher's Note: MDPI stays neutral with regard to jurisdictional claims in published maps and institutional affiliations.



Copyright: © 2022 by the authors. Licensee MDPI, Basel, Switzerland. This article is an open access article distributed under the terms and conditions of the Creative Commons Attribution (CC BY) license (<https://creativecommons.org/licenses/by/4.0/>).

Abstract: Ni-Mn-Sn ferromagnetic shape memory alloys, which can be stimulated by an external magnetic field, exhibit a fast response and have aroused wide attention. However, the fixed and restricted working temperature range has become a challenge in practical application. Here, we introduced strain engineering, which is an effective strategy to dynamically tune the broad working temperature region of Ni-Co-Mn-Sn alloys. The influence of biaxial strain on the working temperature range of Ni-Co-Mn-Sn alloy was systematically investigated by the ab initio calculation. These calculation results show a wide working temperature range (200 K) in Ni₁₄Co₂Mn₁₃Sn₃ FSMAs can be achieved with a slight strain from 1.5% to −1.5%, and this wide working temperature range makes Ni₁₄Co₂Mn₁₃Sn₃ meet the application requirements for both low-temperature and high-temperature (151–356 K) simultaneously. Moreover, strain engineering is demonstrated to be an effective method of tuning martensitic transformation. The strain can enhance the stability of the Ni₁₄Co₂Mn₁₃Sn₃ martensitic phase. In addition, the effects of strain on the magnetic properties and the martensitic transformation are explained by the electronic structure in Ni₁₄Co₂Mn₁₃Sn₃ FSMAs.

Keywords: martensitic transformation; ferromagnetic shape memory alloys; first-principal calculations; Ni-Co-Mn-Sn; strain engineering

1. Introduction

Ni-Mn-Sn ferromagnetic shape memory alloys (FSMAs) with various related magnetic effects, including excellent magnetocaloric effect (MCE) [1,2], extraordinary magnetic shape memory effect (MSME) [3–5], and magnetoresistance effect (MR) [6,7]. These multifunctional properties are attributable to the coupling between the magnetic and structural transitions by the magnetic field [8–10], i.e., magnetic field-induced martensitic transformation (MFIMT). It is the magnetic field-driven shape memory behavior that makes ferromagnetic shape memory alloys different from conventional shape memory alloys, which must be actuated through temperature. The application of magnetic fields is fast and easy, and its fast response to magnetic fields makes this alloy more widely used than conventional shape memory alloys. Moreover, Ni-Mn-Sn FSMAs are cheap, non-toxic, and have simple fabrication processes, which highlights their advantages over conventional shape memory alloys. Although Ni-Mn-Sn FSMAs have so many excellent properties, the relatively narrow working temperature range is still a key drawback in extensive practical application [11,12]. Previous studies have pointed out that the narrow working temperature

of Ni-Mn-Sn alloys is mainly near room temperature or slightly below it [13–20], which is just more beneficial to magnetic solid-state refrigeration. However, for the automotive, manufacturing, and energy exploration industries, the high working temperature region of the alloys is needed [21,22]. Similarly, a working temperature range lower than 270 K is needed for several space solutions [23]. In addition, the working temperature is very sensitive to constituent elements. That is, the working temperature region with fixed components is also fixed, which also increases the difficulty of widening the working temperature region. Therefore, obtaining the adjustable working temperature range is an urgent problem to be solved in Ni-Mn-Sn alloys.

Strain engineering is an efficient method to enhance the properties of functional materials [24–27]. Experimentally, Huang et al. found that uniaxial strain will be an effective means to control thermal effects (such as giant MCE and elastocaloric effects). A significant cooling level of about 4 K is measured when the strain is released [28]. Yang et al. observed that the martensitic transformation temperature (T_M) increased with the increase in uniaxial strain in $\text{Ni}_{43.5}\text{Co}_{6.5}\text{Mn}_{39}\text{Sn}_{11}$ [29]. In addition, Zhao et al. also measured that the refrigerating temperature region increased by 6 K to 10 K in $\text{Ni}_{43}\text{Co}_7\text{Mn}_{39}\text{Sn}_{11}$ films with applying strain [30]. It can be seen that stress engineering is a very effective method to improve many properties of the system. However, few studies have been able to draw on any systematic research on the influence of biaxial strain on the working temperature in the Ni-Mn-Sn system.

The stable MFIMT and the dynamical working temperature are necessary for a tunable broad working temperature region in Ni-Mn-Sn. For a stable MFIMT, the alloys must be ferromagnetic in the austenitic phase (FM) and antiferromagnetic in the martensitic phase (AF) for a stable MFIMT (AFM). For the dynamical working temperature, the alloys need to require two conditions. (1) Both T_M and Curie temperature (T_C) need to be dynamic. (2) Keeping T_M lower than T_C . In addition, from the view of calculations, the large magnetization (ΔM) between the austenitic and martensitic phases is beneficial to the stable MFIMT [5]. The total energy difference (ΔE_{A-M}) between the austenitic phase and martensitic phase and the total energy difference (ΔE_{P-F}) between the ferromagnetic austenitic phase and paramagnetic austenitic phase play important roles in predicting the working temperature in alloys [5,31,32]. The T_M and T_C are increasing with the increase in the ΔE_{A-M} and ΔE_{P-F} , respectively [31,33]. In light of this, we calculated the ΔM , ΔE_{A-M} , and ΔE_{P-F} with the different strains through first-principles calculations. The results show that the value of ΔM of Ni-Mn-Sn alloys is too small to meet the stable MFIMT. Thus, to improve the value of ΔM and ΔE_{P-F} , we choose the method of doping elements (Co to substitute for Ni atoms) [34,35]. In this way, Ni-Co-Mn-Sn alloys not only have a stable MFIMT but also have a dynamic working temperature. It is a high-quality candidate material for dynamically adjusting the working temperature region.

In the present paper, we aim to propose a strategy to adjust the broad working temperature of Ni-Co-Mn-Sn alloys by strain (from 200 K to 370 K). By using the first-principles calculation, the influences of strain on the magnetic properties, the martensitic phase transformation (MPT), and the working temperature of the alloys have been comprehensively studied. According to the results, a small strain can significantly change the working temperature and maintain the stable MFIMT, and the wide working temperature region of 168 K to 330 K can be predicted under strain from 0% to -1.5% in $\text{Ni}_{14}\text{Co}_2\text{Mn}_{13}\text{Sn}_3$ alloys. In addition, we discussed the physical mechanism of magnetic and martensitic transformation of the $\text{Ni}_{14}\text{Co}_2\text{Mn}_{13}\text{Sn}_3$ alloy through the electronic structure.

2. Calculation Method

The Vienna Ab initio Simulation Package (VASP) code is used to reveal the magnetic properties [36,37], phase structures, and electronic structures of Ni-Co-Mn-Sn FSMA. All works were performed on the basis of the density functional theory (DFT). As the exchange–correlation functional, we used the Perdew–Burke–Ernzerhof (PBE) method and the generalized gradient approximation (GGA) [38]. For Ni-Mn-Sn FSMA, a k-mesh of

$3 \times 6 \times 6$ is used for two phases. The cut-off energy is 500 eV. The $L2_1$ austenite structure ($Fm\bar{3}m$) of $Ni_{16}Mn_{13}Sn_3$ with three inequivalent Wyckoff positions (4a, 4b, 8c) is shown in Figure 1a. The Sb and Mn atoms occupy 4a (0, 0, 0) and 4b (0.50, 0.50, 0.50) positions respectively and Ni atoms occupy the 8c ((0.25, 0.25, 0.25) and (0.75, 0.75, 0.75)) sites. In addition, the calculation method used in the transformation process from austenite to martensite is tetragonal distortion. That is, on the premise of keeping the cell volume unchanged, the optimized austenite structure is subjected to lattice distortion with different tetragonal distortion rates c/a so as to obtain the most stable martensite structure. As seen in Figure 1b, we substituted Co atoms for Ni atoms directly in our study, and Mn_{Sn} is the designation for the excess Mn atoms at the deficient Sn atoms. The Mn atoms that remain at their sites are called Mn_{Mn} in the $Ni_{16-x}Co_xMn_{13}Sn_3$ ($x = 0, 1, 2$) FSMA. For both the austenitic and martensitic phases, we calculated two situations: the magnetic properties of $Ni_{16-x}Co_xMn_{13}Sn_3$ ($x = 0, 1, 2$) alloys are FM states and AFM states. The FM configuration was set by magnetic moments of all Mn atoms (Mn_{Sn} and Mn_{Mn}) parallel to each other. AFM configuration was decided by magnetic moments of Mn_{Sn} , which are opposite in the direction of the magnetic moments of the Mn_{Mn} . According to the VASP user manual [39], the calculation of spin polarization requires the parameter $ISPIN = 2$, while the setting of FM and AFM is determined by the parameter $MAGMOM$. Therefore, the spin polarization of both ferromagnets and antiferromagnets can be achieved by VASP. In first-principles calculations, we simulate biaxial strain by changing lattice vectors directly. That is, fixing the lattice constant in the c-axis while relaxing the lattice constants in the a-axis and b-axis. It is worth mentioning that 0% represents no deformation, positive deformation represents stretching, and negative deformation represents compression.

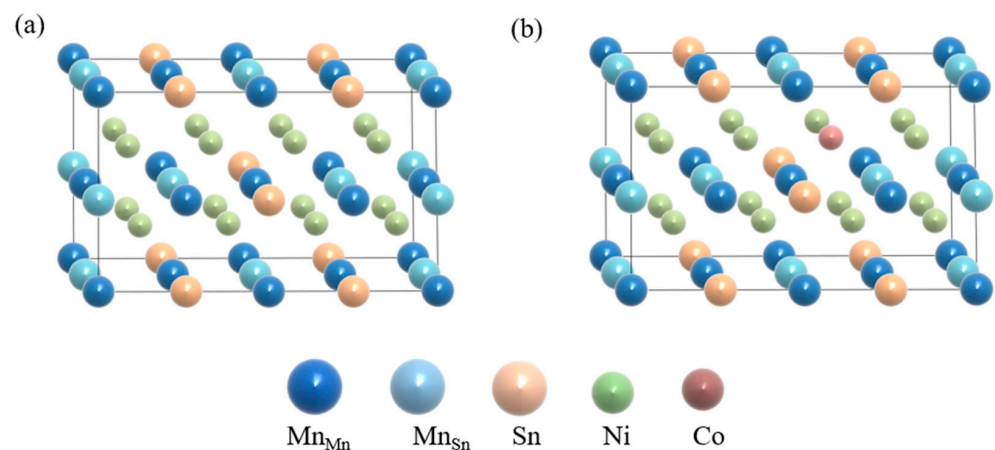


Figure 1. (a) Crystallographic structure in $Ni_{16}Mn_{13}Sn_3$ austenitic phase. (b) Crystallographic structure in $Ni_{15}CoMn_{13}Sn_3$ austenitic phase.

3. Results and Discussion

First, we investigated the two phasic structures, martensitic transition and magnetic properties of the $Ni_{16}Mn_{13}Sn_3$. Table 1 shows the results of our calculations for the magnetic properties and equilibrium lattice parameters of the $Ni_{16}Mn_{13}Sn_3$ alloys. For the $Ni_{16}Mn_{13}Sn_3$ austenitic phase, the AFM state of the alloy is low energy, and the equilibrium lattice parameter is 5.94 Å. The magnetic ground state and lattice constant are in good agreement with other theoretical values [40]. In the $Ni_{16}Mn_{13}Sn_3$ martensitic phase, the FM state has higher energy and is more unstable than the AFM state at $c/a \sim 1.35$. That is, austenite and martensite phase are AFM states under 0% strain. This is also consistent with the theoretical results [3]. According to the energy corresponding to 0% strain in Figure 2, the energy of AFM austenite is higher than that of AFM martensite, so MPT will occur, which is a prerequisite for shape memory alloys. This is also verified experimentally [41]. The above results confirm the correctness of our calculation, so we can apply biaxial strain based on it, and then we calculated the total energies E of the $Ni_{16}Mn_{13}Sn_3$ austenitic phase

and martensitic phase with strain (−1.5~1.5%), as shown in Figure 2a,b respectively, to reveal the effect of strain on the phase structures, MPT, and magnetic properties. Figure 2a indicates that the energy of the AFM state is lower than that in the FM state for the austenite phase, and the total energies E of $\text{Ni}_{16}\text{Mn}_{13}\text{Sn}_3$ austenitic phase firstly decrease with strain from 1.5% to 0% and then increase with strain from 0% to −1.5%. For the $\text{Ni}_{16}\text{Mn}_{13}\text{Sn}_3$ martensitic phase, the total energy E of both FM and AFM increases with strain from 1.5% to −1.5%, and the AFM state energies are lower than the FM state energies. Therefore, we can conclude that austenite and martensite of $\text{Ni}_{16}\text{Mn}_{13}\text{Sn}_3$ alloy are still in AFM state under the application of biaxial strain; that is, the biaxial strain will not affect the magnetic ground state of the system. In addition, the value of ΔE_{A-M} and ΔE_{P-F} in $\text{Ni}_{16}\text{Mn}_{13}\text{Sn}_3$ alloys under strain (−1.5~1.5%) are shown in Figure 3 to show the impact of strain on T_M and T_C . It is obvious that the ΔE_{A-M} increases with strain, while the ΔE_{P-F} decrease with strain under strain from 1.5% to −1.5%. This shows that T_M and T_C increase with the increase in ΔE_{A-M} and ΔE_{P-F} , respectively. According to the results, applying strain can tune the working temperature of $\text{Ni}_{16}\text{Mn}_{13}\text{Sn}_3$ alloys. Based on the above results, it can be concluded that the stability of austenite will be reduced no matter whether biaxial compressive strain or biaxial tensile strain is applied. However, the stability of martensite increases with compressive strain and decreases with tensile strain. Moreover, the biaxial strain does not affect the occurrence of MPT and the most stable magnetic configuration of each phase.

Table 1. Equilibrium lattice parameters, total spin moments and magnetic state of the cubic austenite (Cub.) and tetragonal non-modulated martensite (Tet.) for $\text{Ni}_{16-x}\text{Co}_x\text{Mn}_{13}\text{Sn}_3$ ($x = 0, 1, 2$) alloys with strain (−1.5~1.5%).

Alloys	Strain %	Phase	a Å	c Å	M_t μB	$ \Delta M $ μB	Magnetic State FM/AFM
$\text{Ni}_{16}\text{Mn}_{13}\text{Sn}_3$	−1.5	Cub.	5.85	5.94	1.36	0.06	AFM
		Tet.	5.30	7.26	1.42		AFM
	−1.0	Cub.	5.88	5.94	1.37	0.05	AFM
		Tet.	5.33	7.26	1.42		AFM
	−0.5	Cub.	5.91	5.94	1.38	0.04	AFM
		Tet.	5.35	7.26	1.42		AFM
	0	Cub.	5.94	5.94	1.39	0.04	AFM
		Tet.	5.38	7.26	1.43		AFM
	0.5	Cub.	5.97	5.94	1.40	0.03	AFM
		Tet.	5.41	7.26	1.43		AFM
	1.0	Cub.	6.00	5.94	1.41	0.02	AFM
		Tet.	5.43	7.26	1.43		AFM
	1.5	Cub.	6.03	5.94	1.42	0.01	AFM
		Tet.	5.46	7.26	1.43		AFM
$\text{Ni}_{15}\text{CoMn}_{13}\text{Sn}_3$	−1.5	Cub.	5.83	5.92	1.42	0.02	AFM
		Tet.	5.35	7.06	1.44		AFM
	−1.0	Cub.	5.86	5.92	1.44	0.01	AFM
		Tet.	5.37	7.06	1.45		AFM
	−0.5	Cub.	5.89	5.92	1.44	0.01	AFM
		Tet.	5.40	7.06	1.45		AFM
	0	Cub.	5.92	5.92	1.46	0	AFM
		Tet.	5.43	7.06	1.46		AFM
	0.5	Cub.	5.95	5.92	1.47	0	AFM
		Tet.	5.46	7.06	1.47		AFM
	1.0	Cub.	5.98	5.92	1.49	0.01	AFM
		Tet.	5.48	7.06	1.48		AFM
	1.5	Cub.	6.01	5.92	1.50	0.01	AFM
		Tet.	5.51	7.06	1.49		AFM

Table 1. Cont.

Alloys	Strain %	Phase	a Å	c Å	M_t μB	$ \Delta M $ μB	Magnetic State FM/AFM
$\text{Ni}_{14}\text{Co}_2\text{Mn}_{13}\text{Sn}_3$	−1.5	Cub.	5.84	5.93	6.98	5.48	FM
		Tet.	5.32	7.15	1.50		AFM
	−1.0	Cub.	5.87	5.93	7.00	5.50	FM
		Tet.	5.35	7.15	1.50		AFM
	−0.5	Cub.	5.90	5.93	7.03	5.51	FM
		Tet.	5.37	7.15	1.52		AFM
	0	Cub.	5.93	5.93	7.06	5.54	FM
		Tet.	5.40	7.15	1.52		AFM
	0.5	Cub.	5.96	5.93	7.08	5.56	FM
		Tet.	5.43	7.15	1.52		AFM
	1.0	Cub.	5.99	5.93	7.10	5.58	FM
		Tet.	5.45	7.15	1.52		AFM
	1.5	Cub.	6.02	5.93	7.13	5.58	FM
		Tet.	5.48	7.15	1.55		AFM

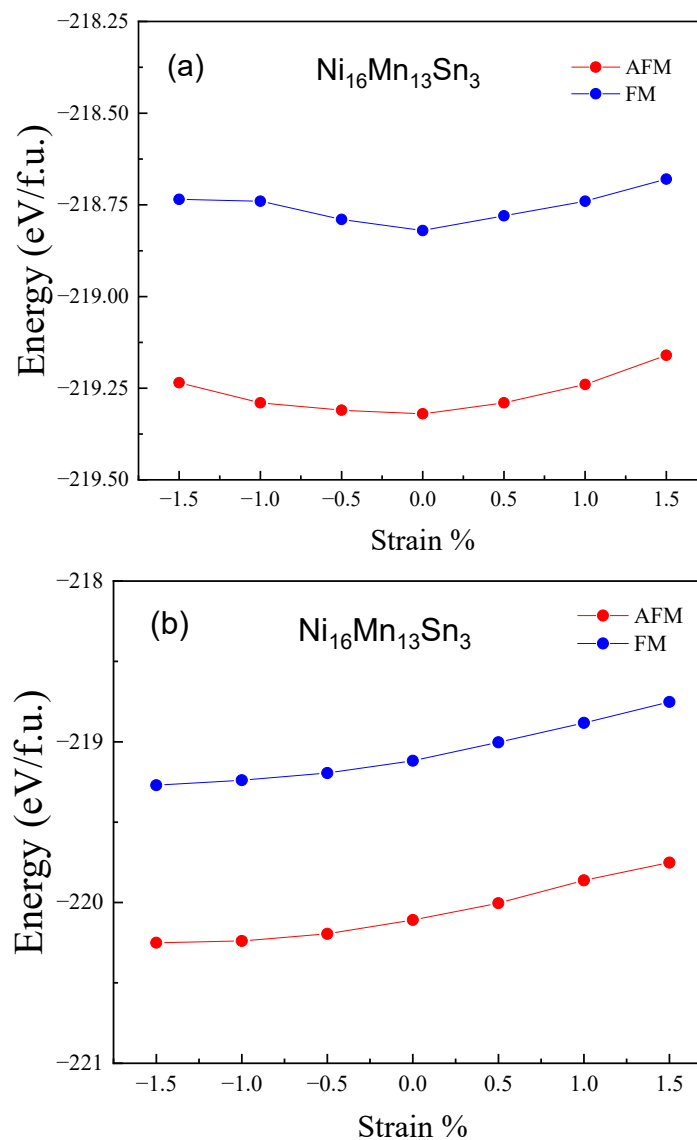


Figure 2. Strain change (−1.5~1.5%) of the total energies of $\text{Ni}_{16}\text{Mn}_{13}\text{Sn}_3$ alloys. (a) the austenitic phase. (b) the martensitic phase.

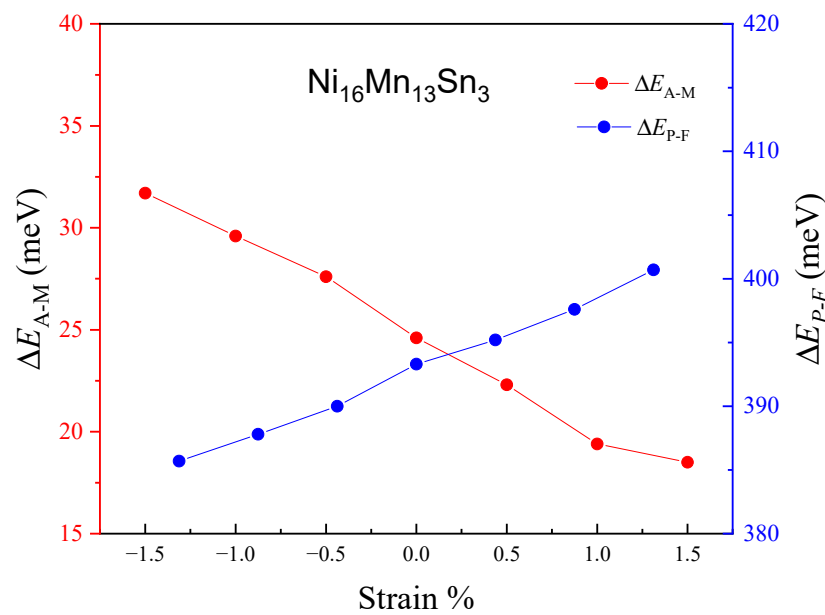


Figure 3. Strain change (−1.5–1.5%) of ΔE_{A-M} and ΔE_{P-F} for $\text{Ni}_{16}\text{Mn}_{13}\text{Sn}_3$.

In order to tune the working temperature of alloys, alloys must have stable MFIMT. The ΔM is larger, and the MFIMT is more stable [41,42]. Therefore, we calculated the ΔM of $\text{Ni}_{16}\text{Mn}_{13}\text{Sn}_3$ alloys with strain in Table 1. Table 1 further accurately shows that the ΔM of $\text{Ni}_{16}\text{Mn}_{13}\text{Sn}_3$ is very small, and the strain has a weak effect on the value of ΔM (0.06–0.01 μB). The low ΔM cannot satisfy the stable MFIMT. Therefore, the biaxial strain alone cannot satisfy the stable MFIMT, which is a necessary condition for an adjusted wide working temperature region. Fortunately, the Co element enhances ferromagnetism in the austenitic phase and T_C of $\text{Ni}_{16}\text{Mn}_{13}\text{Sn}_3$ alloys. Thus, the strain may be an efficacious strategy to adjust the wide working temperature of Ni-Co-Mn-Sn.

The impact of Co doping on the physical properties of the Ni-Co-Mn-Sn system, particularly on the operating temperature, must also be taken into account. We first evaluate the equilibrium lattice parameters and magnetic properties of the $\text{Ni}_{16-x}\text{Co}_x\text{Mn}_{13}\text{Sn}_3$ ($x = 1, 2$) and present them in Table 1 to show the change in phase structures, MPT, and magnetic properties of the $\text{Ni}_{16}\text{Mn}_{13}\text{Sn}_3$ with Co doping. The findings demonstrate that as Co increases, the equilibrium lattice parameters of the $\text{Ni}_{16-x}\text{Co}_x\text{Mn}_{13}\text{Sn}_3$ ($x = 1, 2$) austenitic phases increase from 5.91 Å to 5.93 Å. The change of $\text{Ni}_{16-x}\text{Co}_x\text{Mn}_{13}\text{Sn}_3$ ($x = 1, 2$) lattice constant can be attributed to the fact that the atomic radius of the substitution elements is slightly larger than that of the substituted element, and the lattice parameters are close to the value of the experiment (5.987 Å) and theory (5.973 Å) [43,44]. The origin of the experimental error is the slight difference between the actual compound and the nominal compound, and then the DFT calculation is carried out at $T = 0$ K, while the equilibrium lattice constant measured by XRD is carried out at room temperature. The theoretical error may be caused by the error between different calculation software. The austenitic $\text{Ni}_{14}\text{Co}_2\text{Mn}_{13}\text{Sn}_3$ phase is the FM state, whereas the martensitic phase is the AFM state, and there is a large ΔM (5.48 μB) between these two phases as shown in Table 1. This is also consistent with the experimental facts (6.68 μB) [45]. In short, the $\text{Ni}_{14}\text{Co}_2\text{Mn}_{13}\text{Sn}_3$ alloys meet the stable MFIMT, and the strain method may be an efficient strategy to tune the wide working temperature of $\text{Ni}_{14}\text{Co}_2\text{Mn}_{13}\text{Sn}_3$ alloys.

Subsequently, we calculated the total energies of $\text{Ni}_{14}\text{Co}_2\text{Mn}_{13}\text{Sn}_3$ alloys with strain (−1.5~1.5%) and shown in Figure 4 to show the impact of the magnetic properties and working temperature on this alloy. It is obvious that the total energies of austenitic phases firstly decrease with strain (−1.5~0%) and then increase with strain (0~1.5%), and FM states are the most stable magnetic configuration for austenitic phases. The total energies of martensitic phases increase with strain (−1.5~1.5%), as shown in Figure 4b. Moreover,

the most stable magnetic configuration of martensitic phases is AFM states. Combined with (a) and (b) of Figure 4, it can be seen that the energy of AFM martensite is always less than that of FM austenite under the action of biaxial strain. It shows that the alloy will undergo magnetic structure coupling transformation, which further confirms that there is a large magnetic moment difference in the system. To show the change of T_M and T_C of $Ni_{14}Co_2Mn_{13}Sn_3$ alloys with strain, we listed the ΔE_{A-M} and ΔE_{P-F} in Table 2. The value of ΔE_{A-M} increase with strain from 1.5% to -1.5% , while the value of ΔE_{P-F} decrease with strain from 1.5% to -1.5% . The results show the strain can increase T_M and decrease T_C . In consideration of the wide working temperature of $Ni_{14}Co_2Mn_{13}Sn_3$ alloys, one of the conditions is that T_C must be higher than T_M . Therefore, we need to evaluate the value of T_M and T_C . Generally, the T_M and T_C increase linearly with ΔE_{A-M} and ΔE_{P-F} in Ni-Mn-based Heusler alloys. To further explore the relationship between T_M and ΔE_{A-M} , as depicted in Figure 5, we made the T_M and ΔE_{A-M} fitting curves [1,10,34,35,46–51]. According to the Heisenberg model and Stoner theory [52], the relationship of T_M and ΔE_{A-M} is represented by $\Delta E_{P-F} = -k_B T_C M / M_0$, where M is the magnetic moment at $T \neq 0$ K, and M_0 is the equilibrium magnetic moment at $T = 0$ K [53]. Based on it, we calculated the T_M and T_C of $Ni_{14}Co_2Mn_{13}Sn_3$ alloys with strain in Figure 6. It shows that the T_M and T_C increase with strain, and the T_M is lower than T_C with strain ($-1.5\sim 1.5\%$), which indicates that the alloy has been fully qualified to dynamically adjust the wide working temperature range. In addition, the changing trend of T_M is consistent with the experiment in other Ni-Mn based [54]; that is, the working temperature moves to a high temperature under the compressive strain. Then, with strain from 0% to -1.5% , the $Ni_{14}Co_2Mn_{13}Sn_3$ FSMA's show a tunable wide working temperature (from 168 K to 330 K), which meets the application in different temperatures. The operating temperature range of $Ni_{14}Co_2Mn_{13}Sn_3$ is 160 K; the wide range may be overestimated compared to experimental values. In short, the strain method is an effective way to tune effectively by using the strain approach for $Ni_{14}Co_2Mn_{13}Sn_3$ alloys.

Table 2. Calculated energy difference ΔE_{A-M} in meV/atom between the austenite and martensite phases, ΔE_{P-F} in meV/atom between the paramagnetic and ferromagnetic state, martensite transition temperature T_M and Curie temperature T_C in $Ni_{16-x}Co_xMn_{13}Sn_3$ ($x = 0, 1, 2$) alloys with strain ($-1.5\sim 1.5\%$).

Alloys	Strain %	ΔE_{A-M} (meV/atom)	ΔE_{P-F} (meV/atom)	T_M (K)	T_C (K)
$Ni_{16}Mn_{13}Sn_3$	-1.5	31.7	385.7	405	397
	-1.0	29.6	387.8	378	399
	-0.5	27.6	390.0	353	401
	0	24.6	393.3	314	405
	0.5	22.3	395.2	285	407
	1.0	19.4	397.6	248	409
	1.5	18.5	400.7	236	412
	-1.5	30.8	392.6	394	404
$Ni_{15}CoMn_{13}Sn_3$	-1.0	28.1	395.9	359	407
	-0.5	26.8	397.7	343	409
	0	23.4	398.2	299	410
	0.5	21.6	403.4	276	415
	1.0	18.7	407.3	239	419
	1.5	17.8	410.4	227	422
	-1.5	25.8	399.6	330	411
	-1.0	22.9	402.1	293	414
$Ni_{14}Co_2Mn_{13}Sn_3$	-0.5	19.0	404.8	243	416
	0	13.2	406.9	168	419
	0.5	12.7	410.7	162	423
	1.0	9.8	413.8	125	426
	1.5	7.2	415.7	92	428

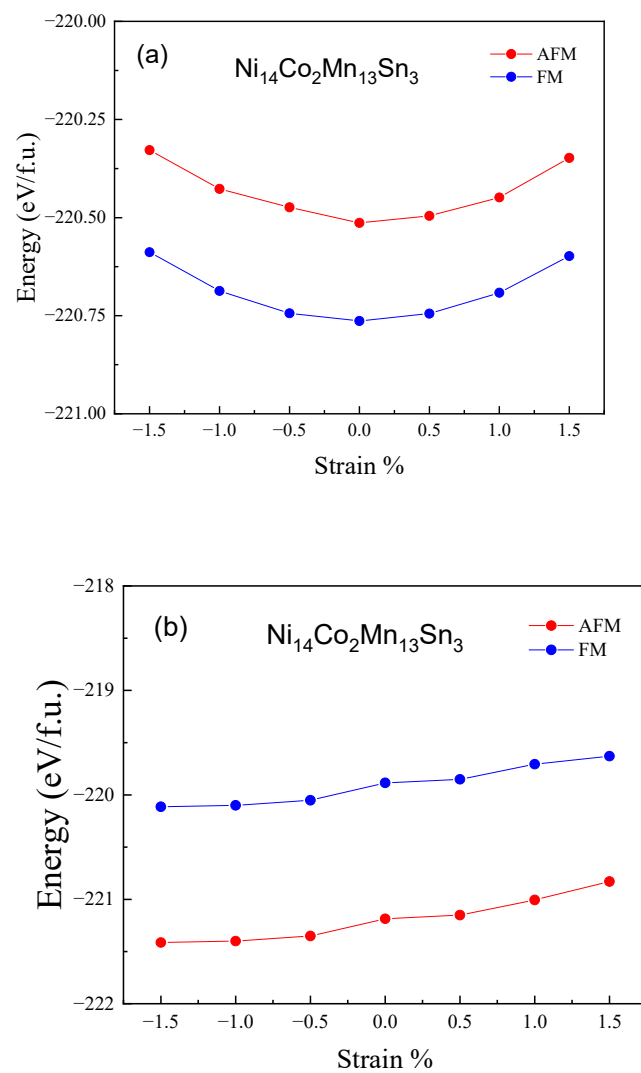


Figure 4. Strain change (−1.5~1.5%) of the total energies of $\text{Ni}_{14}\text{Co}_2\text{Mn}_{13}\text{Sn}_3$ alloys. (a) The austenitic phase. (b) the martensitic phase.

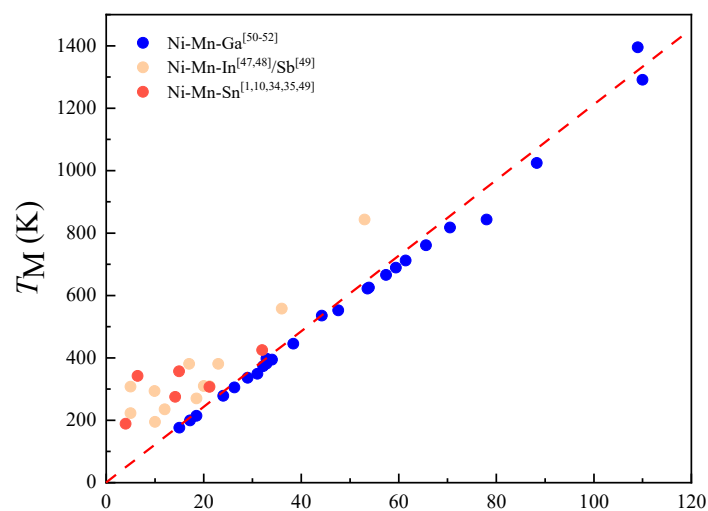


Figure 5. Relationship of ΔE_{A-M} and experimental T_M of alloys.

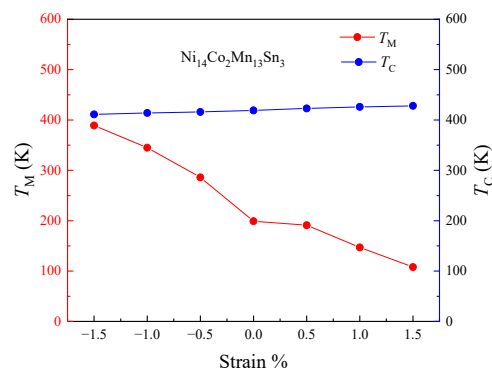


Figure 6. Strain change (−1.5~1.5%) of the T_M and the T_C in $Ni_{14}Co_2Mn_{13}Sn_3$.

The total density of states (TDOS) of austenite and martensite in $Ni_{14}Co_2Mn_{13}Sn_3$ and the partial density of states (PDOS) of Mn_{Mn} and Mn_{Sn} of austenite and martensite in $Ni_{14}Co_2Mn_{13}Sn_3$ are shown in Figures 7–9 respectively to further illuminate the physical mechanism of the MPT and magnetic properties [55,56]. In addition, the phase stability is strongly dependent upon the TDOS at the Fermi level plays (E_F) [57,58]. Usually, the low TDOS indicates the stable phase in $Ni_{14}Co_2Mn_{13}Sn_3$ FSMAs. Figure 7a shows that the TDOS at E_F of strain (−1.5%, 1.5%) is similar in $Ni_{14}Co_2Mn_{13}Sn_3$ austenitic phases. The strain has a weak effect on austenitic phase stability. Moreover, for martensitic phases, the TDOS of −1.5% strain is lower than the TDOS of 1.5% strain at E_F , as shown in Figure 7b. The −1.5% strain decreases the instability of the $Ni_{14}Co_2Mn_{13}Sn_3$ martensitic phase. Then, the instability of the martensitic phase decreases, and the stability of austenitic phases show a few changes. In addition, austenite is a peak at E_F , while martensite is a pseudopotential valley. It shows that the stability of austenite is lower than that of martensite, which leads to the MPT according to the Jahn teller splitting effect. The results show that strain can tune the T_M of $Ni_{14}Co_2Mn_{13}Sn_3$ FSMAs.

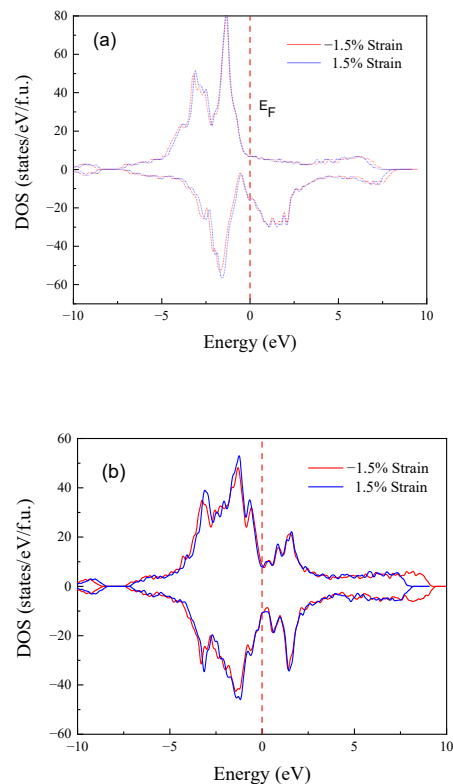


Figure 7. Strain change (−1.5%, 1.5%) of the TDOS of $Ni_{14}Co_2Mn_{13}Sn_3$ alloys. (a) the austenitic phase. (b) the martensitic phase.

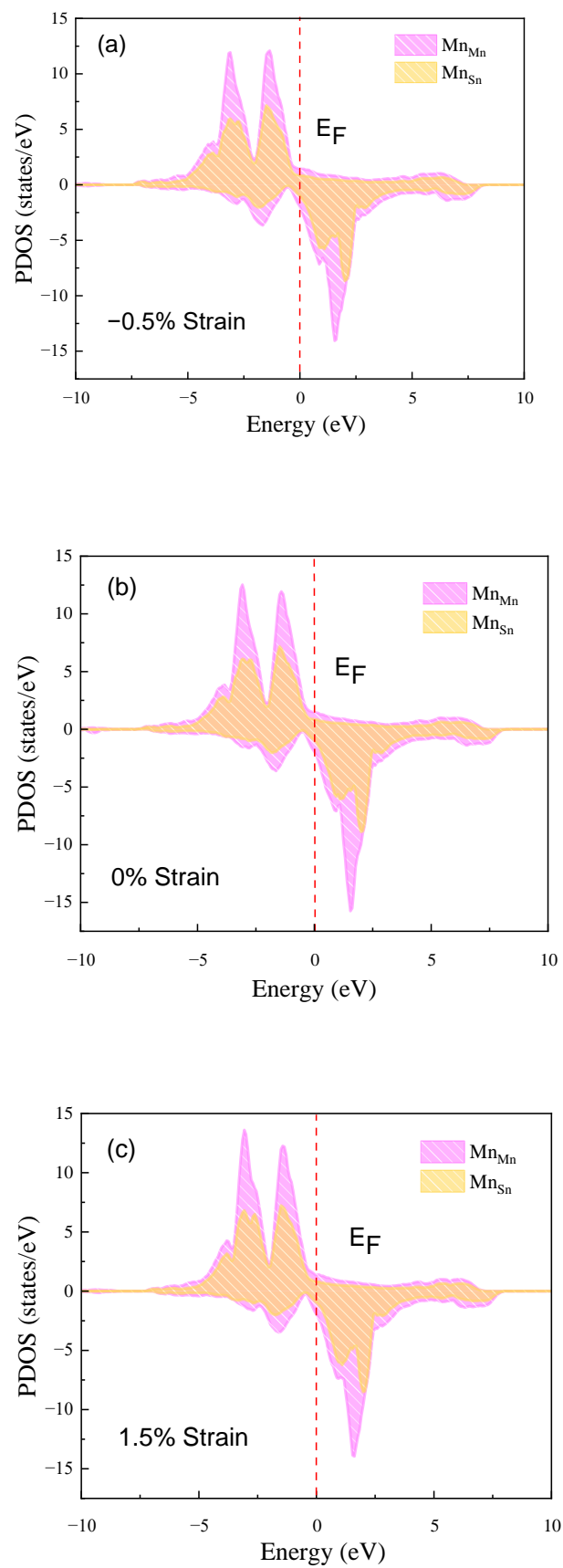


Figure 8. Strain change (−1.5%, 0%, 1.5%) of the PDOS of Ni₁₄Co₂Mn₁₃Sn₃ austenitic phase. (a) −1.5% strain, (b) 0% strain, (c) 1.5% strain.

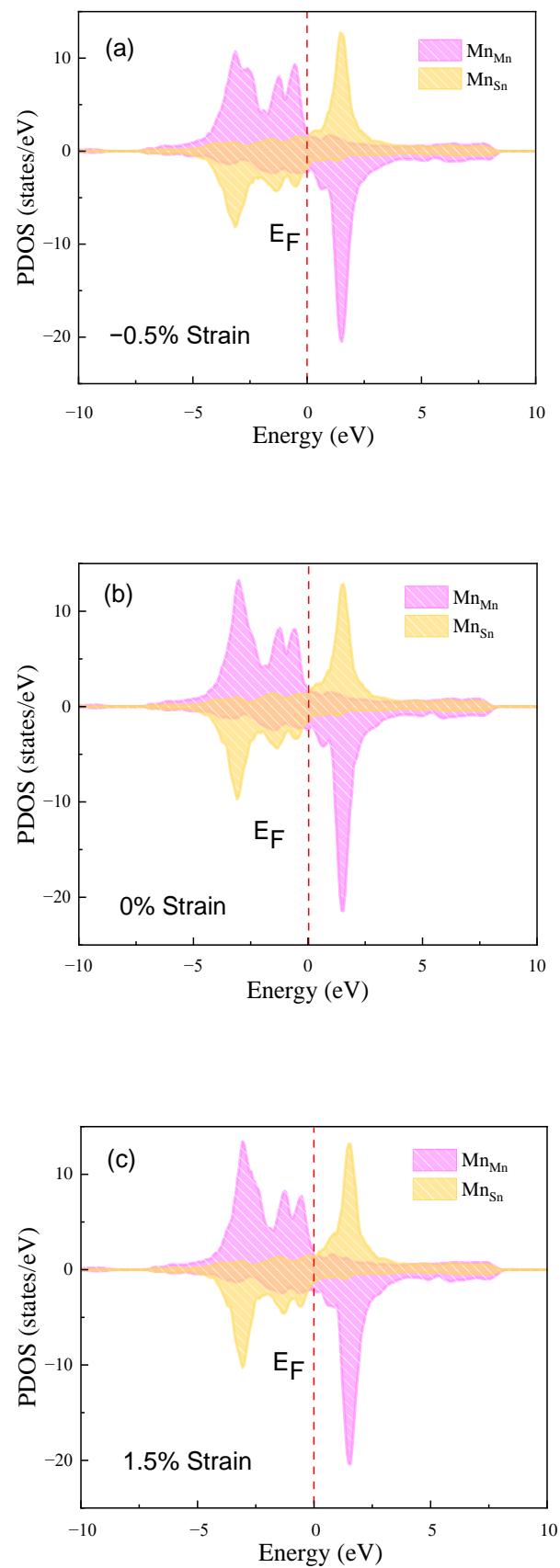


Figure 9. Strain change (−1.5%, 0%, 1.5%) of the PDOS of $\text{Ni}_{14}\text{Co}_2\text{Mn}_{13}\text{Sn}_3$ martensitic phase. (a) −1.5% strain, (b) 0% strain, (c) 1.5% strain.

For the magnetic properties of $\text{Ni}_{14}\text{Co}_2\text{Mn}_{13}\text{Sn}_3$ austenitic phases, as can be seen in Figure 8b, the PDOS of Mn_{Mn} and Mn_{Sn} are similar and mostly up-spin states under the E_{F} . With applying strain, for Figure 8a,c, the PDOS of Mn_{Mn} and Mn_{Sn} has almost no change. This is indicated that the most stable magnetic configuration of austenitic phases is always FM, and this configuration is unaffected by strain. For martensite, in Figure 9b, the Mn_{Mn} is in up-states while the Mn_{Sn} is in down-states. With applying strain, the distribution of the PDOS of Mn_{Mn} and Mn_{Sn} is still different, the Mn_{Sn} is down-state, but the Mn_{Mn} is up-state, as shown in Figure 9a,c. The most stable magnetic configuration of martensite phases is AFM. In addition, the difference in the distribution of austenite and martensite also explains the existence of large ΔM . In conclusion, the strain cannot change the magnetic properties of $\text{Ni}_{14}\text{Co}_2\text{Mn}_{13}\text{Sn}_3$ FSMA. The $\text{Ni}_{14}\text{Co}_2\text{Mn}_{13}\text{Sn}_3$ FSMA meets the condition of the stable MFIMT.

4. Conclusions

To summarize, to achieve the tunable broad working temperature region of Ni-Mn-Sn alloys, we have systematically studied the influence of strain on the structures, MPT, and magnetic properties $\text{Ni}_{16-x}\text{Co}_x\text{Mn}_{13}\text{Sn}_3$ ($x = 0, 1, 2$) by first-principles calculation. The value of $\Delta E_{\text{A-M}}$ increases with the strain from 1.5% to -1.5% , bringing about T_{M} enhancement. According to the results, the strain method can reveal the ability of the tunable wide working temperature range in $\text{Ni}_{14}\text{Co}_2\text{Mn}_{13}\text{Sn}_3$ FSMA. Particularly, with a slight strain ($0\sim 1.5\%$), $\text{Ni}_{14}\text{Co}_2\text{Mn}_{13}\text{Sn}_3$ with a large working temperature region of ~ 160 K and the working temperature ($168\sim 330$ K) of $\text{Ni}_{14}\text{Co}_2\text{Mn}_{13}\text{Sn}_3$ satisfy the application from low-temperature to high-temperature. This work predicts an adjusted broad working temperature region of Ni-Mn-Sn alloys, which shows a great application range of Ni-Mn-Sn FSMA. Therefore, the strain method provides the reference for designing the tunable wide working temperature FSMA and makes it possible for the wide application of FSMA.

Author Contributions: Conceptualization, K.Z.; Data curation, B.H.; Software, L.Z., W.Z., T.M. and C.W.; Writing—original draft, Q.X.; Writing—review & editing, C.T., X.T. and K.Z. All authors have read and agreed to the published version of the manuscript.

Funding: This work was supported by the National Natural Science Foundation of China (Grant No. 51971085, 51871083, 52001101) and the China Postdoctoral Science Foundation (Grant No. 2021M693229).

Institutional Review Board Statement: Not applicable.

Informed Consent Statement: Not applicable.

Data Availability Statement: The data that support the findings of this study are available from the corresponding author upon reasonable request.

Conflicts of Interest: The authors declare no conflict of interest.

References

1. Krenke, T.; Duman, E.; Acet, M.; Wassermann, E.F.; Moya, X.; Mañosa, L.; Planes, A. Inverse magnetocaloric effect in ferromagnetic Ni–Mn–Sn alloys. *Nat. Mater.* **2005**, *4*, 450–454. [[CrossRef](#)] [[PubMed](#)]
2. Han, Z.D.; Wang, D.H.; Zhang, C.L.; Tang, S.L.; Gu, B.X.; Du, Y.W. Large magnetic entropy changes in the $\text{Ni}_{45.4}\text{Mn}_{41.5}\text{In}_{13.1}$ ferromagnetic shape memory alloy. *Appl. Phys. Lett.* **2006**, *89*, 182507. [[CrossRef](#)]
3. Sutou, Y.; Imano, Y.; Koeda, N.; Omori, T.; Kainuma, R.; Ishida, K.; Oikawa, K. Magnetic and martensitic transformations of NiMnX ($X = \text{In, Sn, Sb}$) ferromagnetic shape memory alloys. *Appl. Phys. Lett.* **2004**, *85*, 4358. [[CrossRef](#)]
4. Kainuma, R.; Imano, Y.; Ito, W.; Morito, H.; Sutou, Y.; Oikawa, K.; Fujita, A.; Ishida, K.; Okamoto, S.; Kitakami, O.; et al. Metamagnetic shape memory effect in a Heusler-type $\text{Ni}_{43}\text{Co}_7\text{Mn}_{39}\text{Sn}_{11}$ polycrystalline alloy. *Appl. Phys. Lett.* **2006**, *88*, 192513. [[CrossRef](#)]
5. Kainuma, R.; Imano, Y.; Ito, W.; Sutou, Y.; Morito, H.; Okamoto, S.; Kitakami, O.; Oikawa, K.; Fujita, A.; Kanomata, T.; et al. Magnetic-field-induced shape recovery by reverse phase transformation. *Nature* **2006**, *439*, 957–960. [[CrossRef](#)]
6. Yu, S.Y.; Liu, Z.H.; Liu, G.D.; Chen, J.L.; Cao, Z.X.; Wu, G.H.; Zhang, B.; Zhang, X.X. Large magnetoresistance in single-crystalline $\text{Ni}_{50}\text{Mn}_{50-x}\text{In}_x$ alloys ($x = 14\sim 16$) upon martensitic transformation. *Appl. Phys. Lett.* **2006**, *89*, 162503. [[CrossRef](#)]

7. Koyama, K.; Okada, H.; Watanabe, K.; Kanomata, T.; Kainuma, R.; Ito, W.; Oikawa, K.; Ishida, K. Observation of large magnetoresistance of magnetic Heusler alloy Ni₅₀Mn₃₆Sn₁₄ in high magnetic fields. *Appl. Phys. Lett.* **2006**, *89*, 182510. [[CrossRef](#)]
8. Xuan, H.C.; Cao, Q.Q.; Zhang, C.L.; Ma, S.C.; Chen, S.Y.; Wang, D.H.; Du, Y.W. Large exchange bias field in the Ni–Mn–Sn Heusler alloys with high content of Mn. *Appl. Phys. Lett.* **2010**, *96*, 202502. [[CrossRef](#)]
9. Qu, Y.H.; Cong, D.Y.; Sun, X.M.; Nie, Z.H.; Gui, W.Y.; Li, R.G.; Ren, Y.; Wang, Y.D. Giant and reversible room-temperature magnetocaloric effect in Ti-doped Ni–Co–Mn–Sn magnetic shape memory alloys. *Acta Mater.* **2017**, *134*, 236–248. [[CrossRef](#)]
10. Zheng, H.; Wang, W.; Xue, S.; Zhai, Q.; Frenzel, J.; Luo, Z. Composition-dependent crystal structure and martensitic transformation in Heusler Ni–Mn–Sn alloys. *Acta Mater.* **2013**, *61*, 4648–4656. [[CrossRef](#)]
11. Krenke, T.; Acet, M.; Wassermann, E.; Moya, X.; Mañosa, L.; Plane, A. Martensitic transitions and the nature of ferromagnetism in the austenitic and martensitic states of Ni–Mn–Sn alloys. *Phys. Rev. B* **2005**, *72*, 014412. [[CrossRef](#)]
12. Ghosh, A.; Mandal, K. Effect of structural disorder on the magnetocaloric properties of Ni–Mn–Sn alloy. *Appl. Phys. Lett.* **2014**, *104*, 031905. [[CrossRef](#)]
13. Aguilar-Ortiz, C.O.; Soto-Parra, D.; Álvarez-Alonso, P.; Lázpita, P.; Salazar, D.; Castillo-Villa, P.O.; Flores-Zúñiga, H.; Chernenko, V.A. Influence of Fe doping and magnetic field on martensitic transition in Ni–Mn–Sn melt-spun ribbons. *Acta Mater.* **2016**, *107*, 9–16. [[CrossRef](#)]
14. Machavarapu, R.; Jakob, G. Exchange bias effect in the martensitic state of Ni–Co–Mn–Sn film. *Appl. Phys. Lett.* **2013**, *102*, 957. [[CrossRef](#)]
15. Chatterjee, S.; Giri, S.; De, S.K.; Majumdar, S. Giant magneto-caloric effect near room temperature in Ni–Mn–Sn–Ga alloys. *J. Alloys Compd.* **2010**, *503*, 273–276. [[CrossRef](#)]
16. Wu, Z.; Guo, J.; Liang, Z.; Zhang, Y. Room temperature metamagnetic transformation of a tough dual-phase Ni–Mn–Sn–Fe ferromagnetic shape memory alloy. *J. Alloys Compd.* **2020**, *829*, 154606. [[CrossRef](#)]
17. Moya, X.; Mañosa, L.; Planes, A.; Krenke, T.; Duman, E.; Acet, M.; Wassermann, E.F. Calorimetric study of the inverse magnetocaloric effect in ferromagnetic Ni–Mn–Sn. *J. Magn. Magn. Mater.* **2007**, *316*, 572–574. [[CrossRef](#)]
18. Zhang, K.; Tan, C.; Guo, E.; Feng, Z.; Zhu, J.; Tong, Y.; Cai, W. Simultaneous tuning of martensitic transformation behavior, magnetic and mechanical properties in Ni–Mn–Sn magnetic alloy by Cu doping. *J. Mater. Chem. C* **2018**, *6*, 5228–5238. [[CrossRef](#)]
19. Jing, C.; Li, Z.; Zhang, H.L.; Chen, J.P.; Qiao, Y.F.; Cao, S.X.; Zhang, J.C. Martensitic transition and inverse magnetocaloric effect in Co doping Ni–Mn–Sn Heusler alloy. *Eur. Phys. J. B* **2009**, *67*, 193–196. [[CrossRef](#)]
20. Krenke, T.; Duman, E.; Acet, M.; Moya, X.; Mañosa, L.; Planes, A. Effect of Co and Fe on the inverse magnetocaloric properties of Ni–Mn–Sn. *J. Appl. Phys.* **2007**, *102*, 033903. [[CrossRef](#)]
21. Ma, J.; Karaman, I.; Noebe, R.D. High temperature shape memory alloys. *Int. Mater. Rev.* **2010**, *55*, 257–315. [[CrossRef](#)]
22. Zhang, K.; Tan, C.; Zhao, W.; Guo, E.; Tian, X. Computation-Guided Design of Ni–Mn–Sn Ferromagnetic Shape Memory Alloy with Giant Magnetocaloric Effect and Excellent Mechanical Properties and High Working Temperature via Multielement Doping. *ACS Appl. Mater. Interfaces* **2019**, *11*, 34827–34840. [[CrossRef](#)] [[PubMed](#)]
23. Benafan, O.; Bigelow, G.S.; Garge, A.; Noebe, R.D. Viable low temperature shape memory alloys based on Ni–Ti–Hf formulations. *Scr. Mater.* **2019**, *164*, 115–120. [[CrossRef](#)]
24. Deng, S.; Sumant, A.V.; Berry, V. Strain engineering in two-dimensional nanomaterials beyond grapheme. *Nano Today* **2018**, *22*, 14–35. [[CrossRef](#)]
25. Cao, J.; Zhou, J.; Li, M.; Chen, J.; Zhang, Y.; Liu, X. Insightful understanding of three-phase interface behaviors in 1T-2H MoS₂/CFP electrode for hydrogen evolution improvement. *Chin. Chem. Lett.* **2022**, *33*, 3745–3751. [[CrossRef](#)]
26. Conley, H.J.; Wang, B.; Ziegler, J.I.; Haglund, R.F.; Pantelides, S.T.; Bolotin, K.I. Bandgap Engineering of Strained Monolayer and Bilayer MoS₂. *Nano Lett.* **2013**, *13*, 3626–3630. [[CrossRef](#)]
27. Li, Z.; Lv, Y.; Ren, L.; Li, J.; Kong, L.; Zeng, Y.; Tao, Q.; Wu, R.; Ma, H.; Zhao, B.; et al. Efficient Strain Modulation of 2D Materials Via Polymer Encapsulation. *Nat. Commun.* **2020**, *11*, 1151. [[CrossRef](#)]
28. Huang, Y.J.; Hu, Q.D.; Bruno, N.M.; Chen, J.H.; Karaman, I.; Jr, J.H.R.; Li, J.G. Giant elastocaloric effect in directionally solidified Ni–Mn–In magnetic shape memory alloy. *Scr. Mater.* **2015**, *105*, 42–45. [[CrossRef](#)]
29. Yang, Z.; Cong, D.Y.; Huang, L.; Nie, Z.H.; Sun, X.M.; Zhang, Q.H.; Wang, Y.D. Large elastocaloric effect in a Ni–Co–Mn–Sn magnetic shape memory alloy. *Mater. Des.* **2016**, *92*, 932–936. [[CrossRef](#)]
30. Zhao, X.; Wen, J.; Gong, Y.; Ma, S.; Hu, Q.; Wang, D. Nonvolatile manipulation of the magnetocaloric effect in Ni₄₃Co₇Mn₃₉Sn₁₁/(011)PMN-PT composite by electric fields. *Scr. Mater.* **2019**, *167*, 41–45. [[CrossRef](#)]
31. Dutta, B.; Bhandary, S.; Ghosh, S.; Sanyal, B. First-principles study of magnetism in Pd₃Fe under pressure. *Phys. Rev. B* **2012**, *86*, 024419. [[CrossRef](#)]
32. Chakrabarti, A.; Siewert, M.; Roy, T.; Mondal, K.; Banerjee, A.; Gruner, M.E.; Entel, P. Ab initio studies of effect of copper substitution on the electronic and magnetic properties of Ni₂MnGa and Mn₂NiGa. *Phys. Rev. B* **2013**, *88*, 174116. [[CrossRef](#)]
33. Guillou, F.; Porcari, G.; Yibole, H.; van Dijk, N.; Brück, E. Taming the First-Order Transition in Giant Magnetocaloric Materials. *Adv. Mater.* **2014**, *26*, 2671–2675. [[CrossRef](#)]
34. Cong, D.Y.; Roth, S.; Schultz, L. Magnetic properties and structural transformations in Ni–Co–Mn–Sn multifunctional alloys. *Acta Mater.* **2012**, *60*, 5335–5351. [[CrossRef](#)]
35. Ghosh, A.; Mandal, K. Large magnetoresistance associated with large inverse magnetocaloric effect in Ni–Co–Mn–Sn alloys. *Eur. Phys. J. B* **2013**, *86*, 378. [[CrossRef](#)]

36. Kresse, G.; Furthmüller, J. Efficient iterative schemes for ab initio total-energy calculations using a plane-wave basis set. *Phys. Rev. B* **1996**, *54*, 11169. [[CrossRef](#)]
37. Kresse, G.; Joubert, D. From ultrasoft pseudopotentials to the projector augmented-wave method. *Phys. Rev. B* **1999**, *59*, 1758. [[CrossRef](#)]
38. Perdew, J.P.; Burke, K.; Ernzerhof, M. Generalized gradient approximation made simple. *Phys. Rev. Lett.* **1996**, *77*, 3865. [[CrossRef](#)]
39. VASP Users Guide. Available online: <http://cms.mpi.univie.ac.at/VASP/> (accessed on 7 March 2022).
40. Sokolovskiy, V.; Zagrebin, M.; Buchelnikov, V. First-principles study of Ni-Co-Mn-Sn alloys with regular and inverse Heusler structure. *J. Magn. Magn. Mater.* **2019**, *476*, 546–550. [[CrossRef](#)]
41. Karaca, H.E.; Karaman, I.; Basaran, B.; Lagoudas, D.C.; Chumlyakov, Y.I.; Maier, H.J. On the stress-assisted magnetic-field-induced phase transformation in Ni₂MnGa ferromagnetic shape memory alloys. *Acta Mater.* **2007**, *55*, 4253–4269. [[CrossRef](#)]
42. Dederichs, P.H.; Sato, K.; Katayama-Yoshida, H. Dilute magnetic semiconductors. *Phase Transit.* **2005**, *78*, 851–867. [[CrossRef](#)]
43. Li, C.M.; Hu, Q.M.; Yang, R.; Johansson, B.; Vitos, L. Theoretical investigation of the magnetic and structural transitions of Ni-Co-Mn-Sn metamagnetic shape-memory alloys. *Phys. Rev. B* **2015**, *92*, 024105. [[CrossRef](#)]
44. Bhatti, K.P.; El-Khatib, S.; Srivastava, V.; James, R.D.; Leighton, C. Small-angle neutron scattering study of magnetic ordering and inhomogeneity across the martensitic phase transformation in Ni_{50-x}Co_xMn₄₀Sn₁₀ alloys. *Phys. Rev. B* **2012**, *85*, 134450. [[CrossRef](#)]
45. Buchelnikov, V.; Sokolovskiy, V.; Zagrebin, M.A.; Baygutlin, D. *Large Change of Magnetic Moment in Ni₁₃Co₃Mn₁₃Sn₃ and Ni₁₃Co₃Mn₁₃Sn₂Al₁ Heusler Alloys at Martensitic Transitions: Investigation from First Principles*; IEEE: Piscataway, NJ, USA, 2017.
46. Liu, J.; Scheerbaum, N.; Lyubina, J.; Gutfleisch, O. Reversibility of magnetostructural transition and associated magnetocaloric effect in Ni–Mn–In–Co. *Appl. Phys. Lett.* **2008**, *93*, 102512. [[CrossRef](#)]
47. Sharma, V.K.; Chattopadhyay, M.K.; Chandra, L.S.S.; Roy, S.B. Elevating the temperature regime of the large magnetocaloric effect in a Ni–Mn–In alloy towards room temperature. *J. Phys. D Appl. Phys.* **2011**, *44*, 145002. [[CrossRef](#)]
48. Sánchez-Alarcos, V.; Pérez-Landazábal, J.I.; Recarte, V.; Lucia, I.; Vélez, J.; Rodríguez-Velamazán, J.A. Effect of high-temperature quenching on the magnetostructural transformations and the long-range atomic order of Ni–Mn–Sn and Ni–Mn–Sb metamagnetic shape memory alloys. *Acta Mater.* **2013**, *61*, 4676–4682. [[CrossRef](#)]
49. Yang, X.; Wang, Y.; Du, M.; Xue, Y. First-principles study of Pt doping effects on Ni₂MnGa and Ni₂FeGa ferromagnetic shape memory alloys. *J. Appl. Phys.* **2019**, *126*, 085103. [[CrossRef](#)]
50. Roy, T.; Chakrabarti, A. Possibility of martensite transition in Pt–Y–Ga (Y = Cr, Mn, and Fe) system: An ab-initio calculation of the bulk mechanical, electronic and magnetic properties. *J. Magn. Magn. Mater.* **2016**, *401*, 929–937. [[CrossRef](#)]
51. Ullakko, K.; Huang, J.K.; Kokorin, V.V.; O’Handley, R.C. Magnetically controlled shape memory effect in Ni₂MnGa intermetallics. *Scr. Mater.* **1997**, *36*, 1133–1138. [[CrossRef](#)]
52. Sato, K.; Dederics, P.H.; Katayama-Yoshida, H. Curie temperatures of III–V diluted magnetic semiconductors calculated from first principles. *Europhys. Lett.* **2003**, *61*, 403–408. [[CrossRef](#)]
53. Bai, J.; Raulot, J.; Zhang, Y.; Esling, C.; Zhao, X.; Zuo, L. The effects of alloying element Co on Ni–Mn–Ga ferromagnetic shape memory alloys from first-principles calculations. *Appl. Phys. Lett.* **2011**, *98*, 164103. [[CrossRef](#)]
54. Millán-Solsona, R.; Stern-Taulats, E.; Vives, E.; Planes, A.; Sharma, J.; Nayak, A.K.; Suresh, K.G.; Mañosa, L. Large entropy change associated with the elastocaloric effect in polycrystalline Ni–Mn–Sb–Co magnetic shape memory alloys. *Appl. Phys. Lett.* **2014**, *105*, 241901. [[CrossRef](#)]
55. Liang, X.; Bai, J.; Gu, J.; Wang, J.; Yan, H.; Zhang, Y.; Zuo, L. Ab initio-based investigation of phase transition path and magnetism of Ni–Mn–In alloys with excess Ni or Mn. *Acta Mater.* **2020**, *195*, 109–122. [[CrossRef](#)]
56. Wang, J.; Bai, J.; Gu, J.; Yan, H.; Zhang, Y.; Esling, C.; Zuo, L. Investigation of martensitic transformation behavior in Ni–Mn–In Heusler alloy from a first-principles study. *J. Mater. Sci. Technol.* **2020**, *58*, 100–106. [[CrossRef](#)]
57. Ye, M.; Kimura, A.; Miura, Y.; Shirai, M.; Cui, Y.T.; Shimada, K.; Kanomata, T. Role of electronic structure in the martensitic phase transition of Ni₂Mn_{1+x}Sn_{1-x} studied by hard-X-ray photoelectron spectroscopy and ab initio calculation. *Phys. Rev. Lett.* **2010**, *17*, 176401. [[CrossRef](#)]
58. Zeng, Q.; Shen, J.; Zhang, H.; Chen, J.; Ding, B.; Xi, X.; Liu, E.; Wang, W.; Wu, G. Electronic behaviors during martensitic transformations in all-d-metal Heusler alloys. *J. Phys. Condens. Matter* **2019**, *31*, 425401. [[CrossRef](#)]